

**MICROSTRUCTURAL ASPECTS OF IRRADIATION DAMAGE IN A508 Gr 4N FORGING STEELS:
COMPOSITION & FLUX EFFECTS**

M. G. Burke, R. J. Stofanak, J. M. Hyde, C. A. English and W. L. Server

DE-AC11-98PN38206

NOTICE

This report was prepared as an account of work sponsored by the United States Government. Neither the United States, nor the United States Department of Energy, nor any of their employees, nor any of their contractors, subcontractors, or their employees, makes any warranty, express or implied, or assumes any legal liability or responsibility for the accuracy, completeness or usefulness of any information, apparatus, product or process disclosed, or represents that its use would not infringe privately owned rights.

BETTIS ATOMIC POWER LABORATORY

WEST MIFFLIN, PENNSYLVANIA 15122-0079

**Operated for the U.S. Department of Energy
by Bechtel Bettis, Inc.**

Mary Grace Burke,¹ Raymond J. Stofanak,¹ Jonathan M. Hyde,² Colin A. English² and William L. Server³

Microstructural Aspects of Irradiation Damage in A508 Gr 4N Forging Steel: Composition & Flux Effects

Burke, M. G., Stofanak, R. J., Hyde, J. M., English, C. A., Server, W. L.,
“Microstructural Aspects of Irradiation Damage in A508 Gr 4N Forging Steel: Composition & Flux Effects,” *Effects of Radiation on Materials, ASTM STP 1447*, M. L. Grossbeck and R. G. Lott, Eds., American Society for Testing and Materials, West Conshohocken, PA 2002.

Abstract: Neutron irradiation can promote significant changes in the microstructure and associated mechanical properties of low alloy steels. In particular, irradiation can induce the formation of non-equilibrium phases and segregation, which may lead to a degradation in toughness. In this study, the microstructural changes caused by neutron irradiation have been characterized in A508 Grade (Gr) 4N-type steels (~3.5% Ni) using a variety of state-of-the-art analytical techniques including 3D-Atom Probe Field-Ion Microscopy and Small Angle Neutron Scattering, along with post-irradiation annealing studies combining Positron Annihilation Lineshape Analysis and hardness measurements. Important differences between conventional and “superclean” A508 Gr 4N steel have been identified in this investigation. The data indicate that Ni is not the controlling factor in the irradiation damage behavior of these materials; rather, the Mn content of the steel is a dominant factor in the irradiation-induced microstructural development of solute-related hardening features.

Keywords: Irradiation damage, atom probe field-ion microscopy, small angle neutron scattering, positron annihilation, post-irradiation annealing, Ni effects, Mn effects, solute-related hardening, A508 Gr 4N steel.

Introduction

Considerable research into the area of irradiation damage behavior of low alloy steel has focused on the significant role of alloy composition in controlling the irradiation damage behavior of the material. Numerous empirical studies have been performed to determine the role of various solutes such as Cu, Ni, and P in the irradiation-induced embrittlement of low alloy steels and welds.[1-6] This embrittlement is manifested in an increase in the Charpy ductile-to-brittle transition temperatures and a decrease in the Charpy upper shelf energy of the steel, and is associated with an increase in hardness of

¹ Advisory Scientist and Senior Engineer, respectively, Bettis Atomic Power Laboratory, West Mifflin, PA 15122

² Team Leader and Consultant, respectively, AEA Technology, Didcot, OX., UK

³ President, ATI Consulting, Pinehurst, NC

the material. These irradiation-induced changes in mechanical properties of low alloy steels have been associated with subtle, ultra-fine-scale changes in the microstructure, such as the formation of diffuse solute-enriched “clusters” or “precipitates”, which have been identified by atom probe field-ion microscopy [7,8]. By understanding how neutron irradiation affects the microstructures of structural steels, it should be possible to predict how material variables, such as alloying elements, affect the material’s susceptibility to irradiation damage and embrittlement.

The ASTM A508 Gr 4N (~ 3.3Ni) forging steels are characterized by a bainitic microstructure and exhibit excellent toughness in the quenched and tempered condition. Studies in the literature [4,7] have indicated that steels with high Ni contents (>~1%) are susceptible to enhanced irradiation damage. However, despite the high Ni level in A508 Gr 4N steels, it has been reported that neutron irradiation does not promote enhanced degradation in the 47J transition temperature [9,10]. To understand the irradiation damage behavior of these steels, a detailed microstructural characterization program was performed to identify the changes in microstructure caused by neutron irradiation. A comprehensive study combining 3D-Atom Probe Field-Ion Microscopy (3D-APFIM), Small Angle Neutron Scattering (SANS), Post-Irradiation Annealing (PIA) experiments involving both Positron Annihilation Lineshape Analysis (PALA) and Vickers Hardness Number (VHN) measurements has been performed to acquire the fine-scale morphological and chemical information that is required to properly assess the effects of irradiation on the microstructure of structural steels. Each technique provides unique and specific information that is complementary to the information provided by the other techniques. With such an approach, the role of various solutes, such as Ni and Mn in the development of the irradiation-induced microstructure can be identified.

Experimental: Materials and Techniques

The steels examined in this investigation included two conventional A508 Gr 4N steels and one “superclean” A508 Gr 4N steel, the compositions of which are listed in Table 1. The major difference between the conventional and “superclean” variants is the reduction in Mn level from 0.3 to 0.02 wt.%, and the very low levels of Si, P, and other tramp elements, as discussed in Reference [9]. A508 Gr 4N steels are typically quenched from 927°C followed by tempering at ~615°C for 20 to 50 h. After tempering, these steels were stress-relieved at 565°C for 50 h, and slowly cooled to room temperature.

The steels were irradiated under high flux conditions ($\sim 10^{-7}$ dpa/s) at 239°C to a damage level of 0.017-0.018 dpa. For comparison purposes, one of the steels irradiated under low flux conditions ($\sim 10^{-10}$ dpa/s) at ~ 265°C was also evaluated to explore the effect of dose rate on the irradiation damage response of the steel. Table 2 contains the irradiation conditions and observed 47J Charpy Transition Temperature Shift.

To assess the effect of neutron irradiation on the microstructure, both irradiated and unirradiated archive specimens were characterized by 3D Atom Probe Field-Ion Microscopy (3D-APFIM), Small Angle Neutron Scattering (SANS), and Positron Annihilation Lineshape Analysis (PALA). The 3D-APFIM analyses permitted the identification (composition and size) of any irradiation-induced solute-related hardening

features within the microstructure. Statistical analysis of the 3D-APFIM datasets provided further information concerning subtle irradiation-induced microchemical changes in the materials, such as the development of non-random distributions of solute (solute fluctuations) as well as the development of solute co-segregation. These analyses were performed using the University of Oxford Energy-Compensated Optical Position Sensitive Atom Probe. The SANS analyses coupled with the 3D-APFIM microchemical data enabled the determination of the average size and number density of irradiation-induced scattering centers in bulk specimens. The SANS analyses were performed using the 35 meter D11 instrument in the Institut Laue Langevin (ILL) High Flux Reactor, Grenoble (France). Scattering data were obtained in zero field, $Q \parallel H$, and $Q \perp H$ (field of 1 Tesla). For the SANS data analysis, it was assumed that the scattering centers were spherical and partially-magnetic. Furthermore, based on 3D-APFIM data reported in reference [8], a composition of Fe – 20 Ni – 10 Mn + vacancies was assumed as the composition for the irradiation-induced scattering features. Cu was not included in the composition because the very low bulk levels made it difficult to detect significant enhancement in the clusters. The volume fraction of the irradiation-induced features was also estimated from the $Q \perp H$, assuming a nominal contrast factor of 10^{28} m^{-4} , to obtain a *relative* measure of the irradiation-induced scattering features and permit a comparison with the other irradiated A508 Gr 4N steels.

The Positron Annihilation technique can provide information on the presence of irradiation-induced vacancy-related damage in materials. The increase in vacancy-related defects due to irradiation is associated with an increase in probability that the positrons will be annihilated by conduction electrons as opposed to valence electrons. This leads to a decrease in the width of the γ -ray energy spectral peak and an increase in the PALA S parameter. For this investigation, the difference in PALA S parameter between the irradiated and unirradiated materials was measured. These experiments included post-irradiation anneals (PIA) for 0.5 hour at 260°C, 300°C, 350°C, 400°C and 450°C to monitor the change in PALA response of the materials. These experiments can provide evidence for vacancy-related matrix damage, and the relative stability of this damage. By coupling the PALA-PIA experiments with bulk (20 kg load) measurements of Vickers Hardness Number (VHN) of the steels, the hardening associated with neutron irradiation could be measured, as could the “recovery” of the irradiation-induced vacancy-related damage as a function of post-irradiation annealing. As the temperature increases, the vacancy-related damage “anneals out”, and the hardness will decrease. In the absence of other irradiation-induced hardening features (such as solute-enriched “clusters” or “precipitates”), the hardness after PIA will approach that of the unirradiated sample.

Results

General Baseline Microstructural Analysis

The microstructure of the conventional and “superclean” A508 Gr 4N steels consisted of a fine bainitic lath structure with both intra- and inter-lath carbides, Figure 1.

Table 1 – A508 Gr 4N *Steel Compositions (wt.%)*

Steel	C	Mn	Ni	Si	Cr	Mo	Cu	P	S	Fe
207N947	0.21	0.3	2.89	0.05	1.76	0.46	0.10	0.005	0.005	bal
124S285	0.11	0.33	3.35	0.03	1.82	0.47	0.05	0.007	0.005	bal
Superclean 118K001	0.22	0.02	3.53	0.01	1.79	0.55	0.03	0.003	0.001	bal

Table 2 - *Specimen Irradiation History and Properties*

Steel	Irradiation Temperature	Dose (dpa)	Dose Rate dpa/s	ΔNDT (C-deg)	ΔVHN
207N947	~239°C	0.018	~ 10 ⁻⁷	68	~ 45
124S285	~239°C	0.017	~ 10 ⁻⁷	58	~ 45
	~265°C	0.011	~ 10 ⁻¹⁰	0	~ 10
Superclean 118K001	~239°C	0.018	~ 10 ⁻⁷	21	~ 14

Table 3 – *Summary of Irradiated Material Characterization*

Steel	3D-APFIM	SANS	PIA/ PALA	PIA/VHN
207N947 <i>high φ</i>	Ni and Mn solute fluctuations; Mn-Ni, Ni-Cu, Mn-Si, and Ni-Si co-segregation (0.1% significance); Cu-Si co-segregation (5% significance)	1.1 nm “features” ~9 x 10 ²⁴ /m ³	full recovery of vacancy-related damage at 450°C (started at 350°C)	~30 VHN recovery at 450°C
124S285 <i>high φ</i> <i>low φ</i>	Ni and Mn solute fluctuations; Mn-Ni and Ni-Si cosegregation (0.1% significance); Mn-Si co-seg. (1% significance); Cu-Si and Cu-Ni co-seg. (5% significance)	1.1 nm “features” ~10 ²⁵ /m ³	full recovery of vacancy-related damage at 450°C (started at 350°C)	~30 VHN recovery at 450°C
	Ni and Mn solute fluctuations	<i>Too small for analysis</i>	no recovery; no vacancy-related damage (?)	no recovery
Superclean 118K001 <i>high φ</i>	increase in Ni fluctuations Ni-Si co-segregation (0.1% significance); Cu-Si co-segregation (5% significance)	1.4 nm “features” ~6 X 10 ²³ /m ³	full recovery of vacancy-related damage at 450°C (started at 350°C)	complete recovery

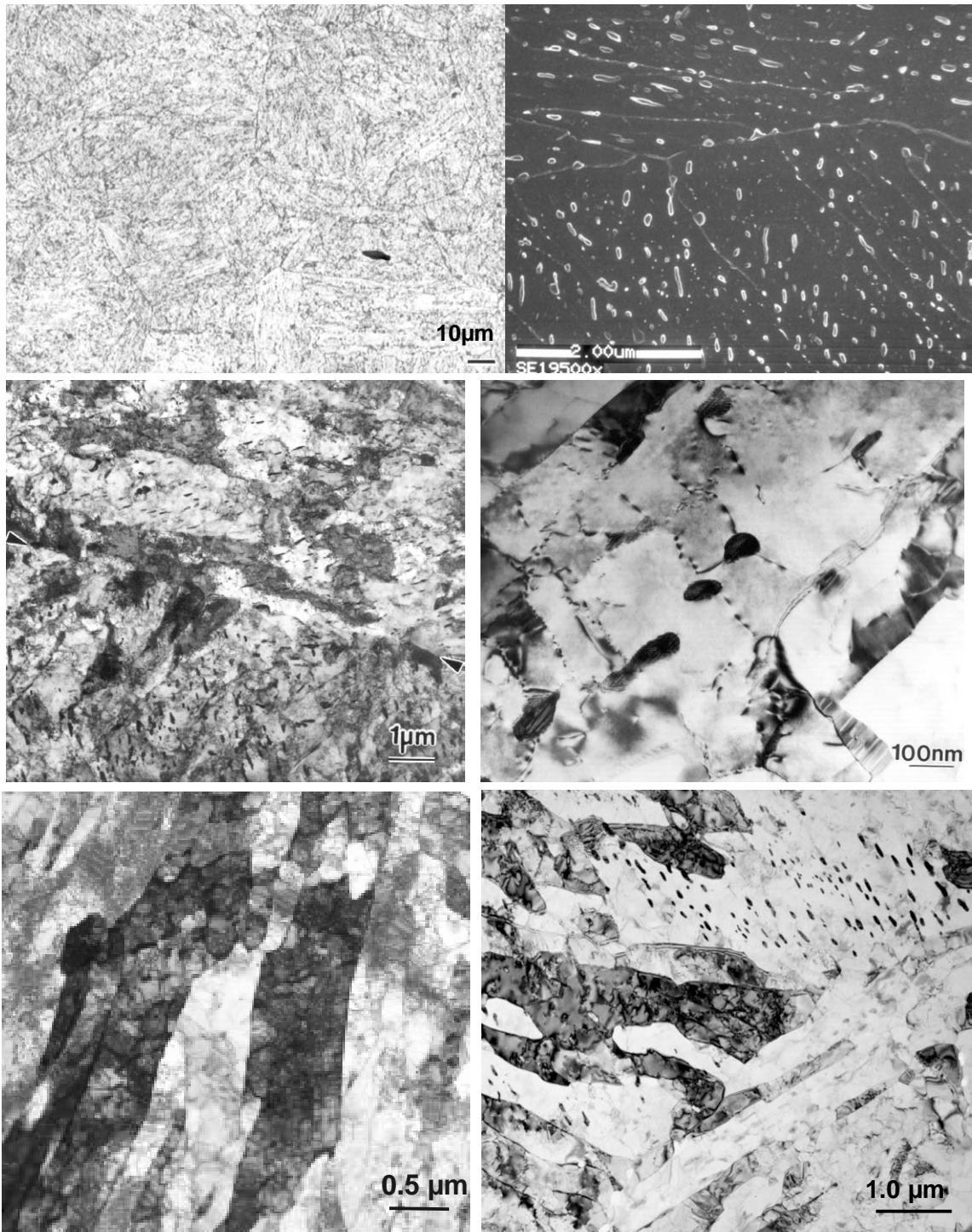


Figure 1 - (a) Light optical micrograph, (b) secondary electron image with the brightly-imaging inter- and intralath carbides, and (c, d) TEM images showing the fine lath structure and extensive carbide precipitation in steel 207N947. (e,f) TEM images of the superclean steel 118K001 showing the bainitic lath structure with carbides.

The carbides were identified by electron diffraction and STEM-EDS microanalysis as Fe-rich M_3C and Cr-rich M_7C_3 , with some Mo-rich M_2C . Some areas of what appeared to be granular bainite were also observed via TEM. Representative micrographs of the conventional and “superclean” A508 Gr 4N are shown in Figure 1.

Characterization of the Irradiation-Induced Microstructures

The results of the 3D-APFIM, SANS, PALA and PIA studies are summarized in Table 3, and are described in the following sections for each steel.

Steel 207N947 (2.9 Ni – 0.3 Mn) irradiated to 0.018 dpa (high flux) - No irradiation-induced solute-enriched “clusters” such as those reported in irradiated commercial A533B-type steels and welds [2,4,7] were observed in this steel. As opposed to the nanoscale Cu-Ni-Mn-Si-Fe “clusters” previously reported in commercial steels, detailed statistical analysis of the 3D-APFIM data using composition frequency distributions [11] revealed the presence of statistically significant (significant at the 0.1% level) Ni and Mn solute fluctuations throughout the analysis volume for this steel. Less pronounced fluctuations in Ni (significant at the 10% level) and Mn (significant at the 5% level) were detected in the unirradiated archive specimen. Further analysis of the 3D-APFIM using the contingency table analysis technique [11] provided evidence of co-segregation of certain elements. Specifically, statistically significant (at the 0.1% level) co-segregation of Ni and Mn, Mn and Si, Ni and Si, and Ni and Cu were observed in the irradiated material. A lesser extent of co-segregation (at the 5% significance level) was observed for Cu and Si.

SANS analysis provided an estimate of the average diameter and number density of the irradiation-induced scattering features within the steel, subject to the constraints of the assumptions described in the Experimental section (i.e., spherical scattering centers, partially-magnetic features with a composition of Fe – 20 Ni – 10 Mn + vacancies). These results are shown in Table 3. The SANS data indicated the presence of very small scattering features, with an average diameter of ~1.1 nm, a volume fraction of ~5%, and a number density of $\sim 9 \times 10^{24}/m^3$.

PALA S parameter measurements of the irradiated and archive specimens confirmed the presence of vacancy-related damage in the irradiated steel. Figure 2 shows the results of the PIA-PALA-VHN analyses. A notable decrease in PALA ΔS parameter and ΔVHN was observed as the post-irradiation annealing temperature increased, with full recovery of the vacancy-related matrix damage at approximately 400°C. Despite the elimination of the irradiation-induced vacancy-related damage (as confirmed by the PALA ΔS parameter) the hardness did not fully recover to the archive value: a residual irradiation-induced hardness increment was still evident.

To further examine the irradiation-induced microstructural changes and their stability during post-irradiation annealing, specimens that had been post-irradiation annealed at 350°C and 450°C were characterized using 3D-APFIM; additional SANS analyses were also performed on the material annealed at 350°C. The results of the 3D-APFIM composition frequency distribution and contingency table analyses revealed that

the Mn and Ni solute fluctuations were still present after the 350°C anneal, even though the PALA ΔS parameter showed that the vacancy-related damage had been significantly reduced (~90%). This anneal resulted in a decrease in the spatial correlation between Ni and Mn, but the extent of co-segregation of Ni and Si, and Ni and Cu remained unchanged. SANS data obtained from this material condition showed a similar ~90% reduction in the volume fraction of scattering features, and some evidence for a slight increase in size of those remaining scattering features. The 3D-APFIM analyses showed that post-irradiation annealing at 450°C did not eliminate the Mn and Ni solute fluctuations, although full recovery of the PALA ΔS parameter indicated complete elimination of the vacancy-related matrix damage. The extent of spatial correlation between the solutes had decreased, with the exception of Mn and Si, and Mn and Cu, which increased slightly.

Steel 124S285 (3.35 Ni – 0.3 Mn) irradiated to 0.017 dpa (high flux)- Similar to steel 207N947, this steel was characterized by the presence of Mn and Ni solute fluctuations, identified via statistical analysis of 3D-APFIM data, and no solute-enriched “clusters” were detected in the matrix. Contingency table analysis of the 3D-APFIM data confirmed that the Mn and Ni were co-segregated at the 0.1% significance level, as were Ni and Si. Mn-Si cosegregation was detected (significance of 1%), whereas Cu-Ni and Cu-Si cosegregation had a significance of 5%. Analysis of the SANS data yielded an average scattering feature size of ~1.1 nm, and number density of $\sim 10^{25}/\text{m}^3$, similar to steel 207N947. PALA ΔS parameter measurements between the as-irradiated and archive samples confirmed the presence of measurable vacancy-related matrix damage. These irradiation-induced microstructural changes were accompanied by an increase of approximately 45 VHN over the unirradiated archive value.

The results of the PALA ΔS parameter and VHN measurements as a function of PIA are presented in Figure 3. Post-irradiation annealing promoted significant recovery of the vacancy-related matrix damage, as measured by the PALA ΔS parameter, with nearly complete recovery observed after 0.5h at 350°C, and full recovery after the 400°C anneal. Although significant recovery of the irradiation-induced hardness was noted after the anneals at 350°C and above, the residual irradiation-induced hardness was ~ 15 VHN after complete elimination of the vacancy-related matrix damage.

Steel 124S285 (3.35 Ni – 0.3 Mn) irradiated to 0.01 dpa (low flux)- 3D-APFIM characterization of this material revealed the presence of Mn and Ni solute fluctuations, similar to those detected in the high-flux irradiated specimens. Less pronounced fluctuations in Ni (significance of 10%) were observed in the unirradiated material, compared to the Ni fluctuations in the low flux irradiated steel (significance of 0.1%). However, in contrast to the co-segregation measured in the high-flux irradiated steels, no co-segregation was observed in this material. In addition, PALA ΔS parameter measurements showed that the presence of vacancy-related matrix damage was insignificant. Similarly, the SANS data failed to show measurable irradiation-induced scattering features in this material. A small increase in hardness due to neutron irradiation was measured (~10 VHN). Post-irradiation annealing did not lead to full recovery of the irradiation-induced hardness, as shown in Figure 4.

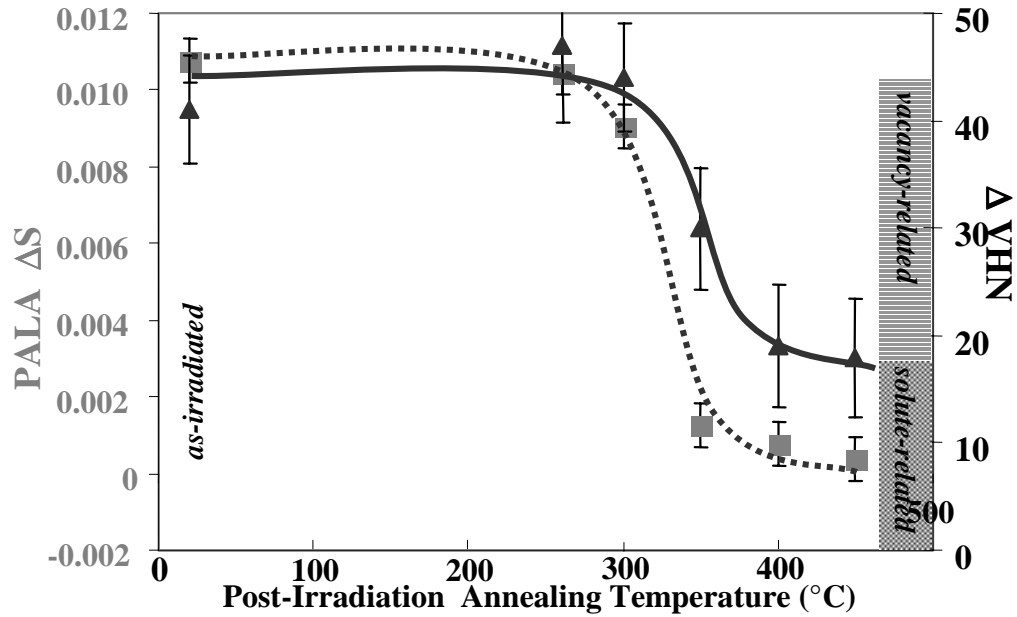


Figure 2 - Effect of PIA on the recovery of the vacancy-related matrix damage in steel 207N94 irradiated to 0.018 dpa as measured by the PALA ΔS parameter (■), and on the irradiation-induced hardness increment (ΔVHN – ▲). The elimination of the vacancy-related damage is associated with a significant decrease in hardness, but there is still significant residual hardness due to Mn and Ni solute fluctuations. The stacked bar at the right indicates the relative contributions of vacancy-related matrix damage and solute-related hardening features to the total irradiation-induced hardening increments.

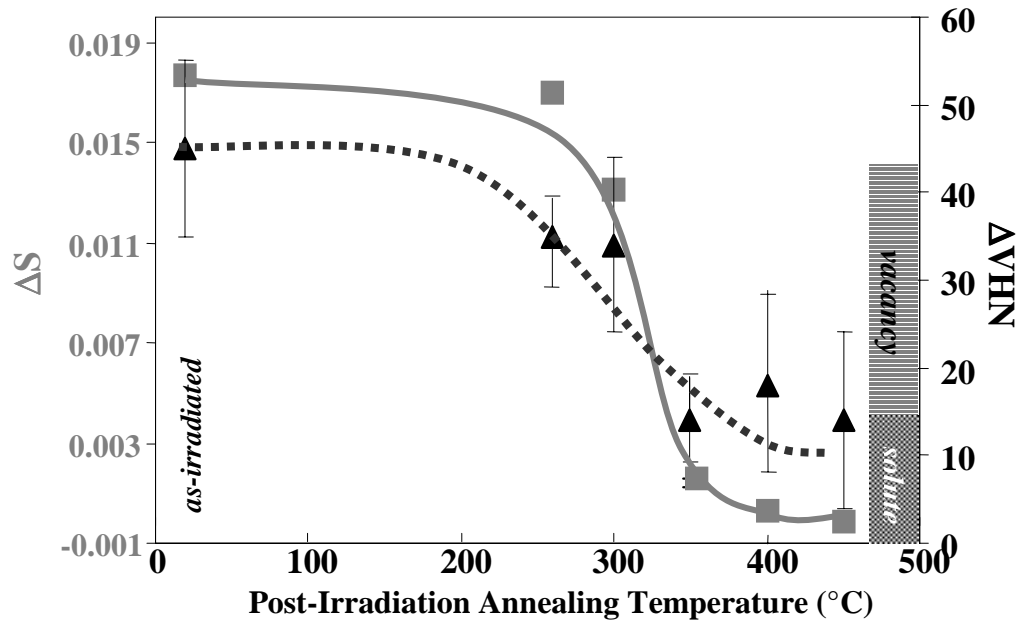


Figure 3 - Effect of PIA on the recovery behavior steel 124S285 irradiated under high-flux conditions to 0.017 dpa. The elimination of the vacancy-related damage (PALA ΔS – ■) resulted in a significant decrease in irradiation-induced hardness (ΔVHN – ▲), but some residual hardness due to solute fluctuations remained.

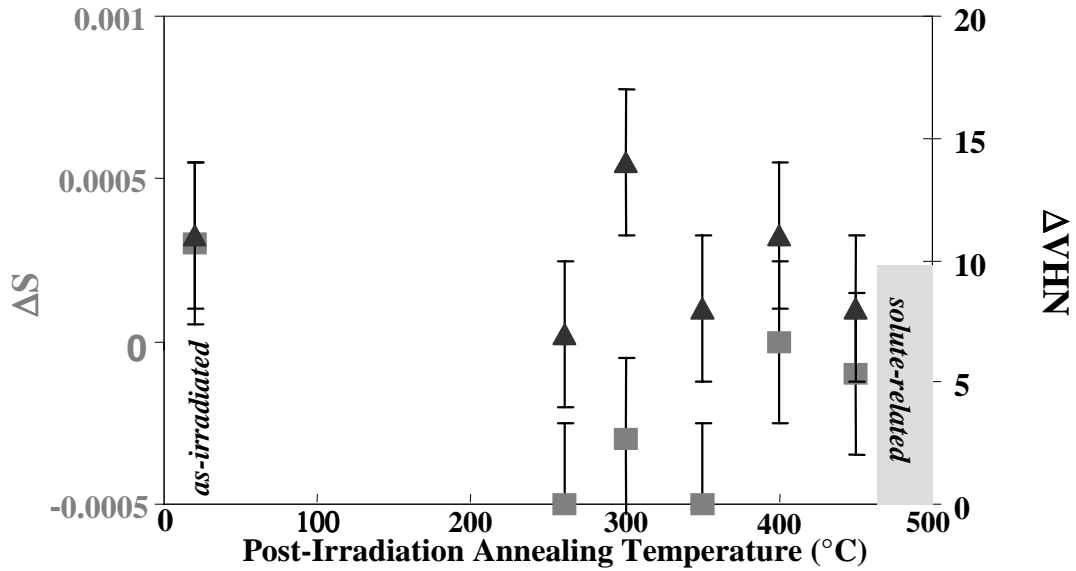


Figure 4 - Effect of PIA on the recovery of the irradiation-induced vacancy-related damage (as characterized by the PALA ΔS parameter - ■) and irradiation-induced Vickers hardness (ΔVHN - ▲) for steel 124S285 irradiated under low-flux conditions to 0.011 dpa.

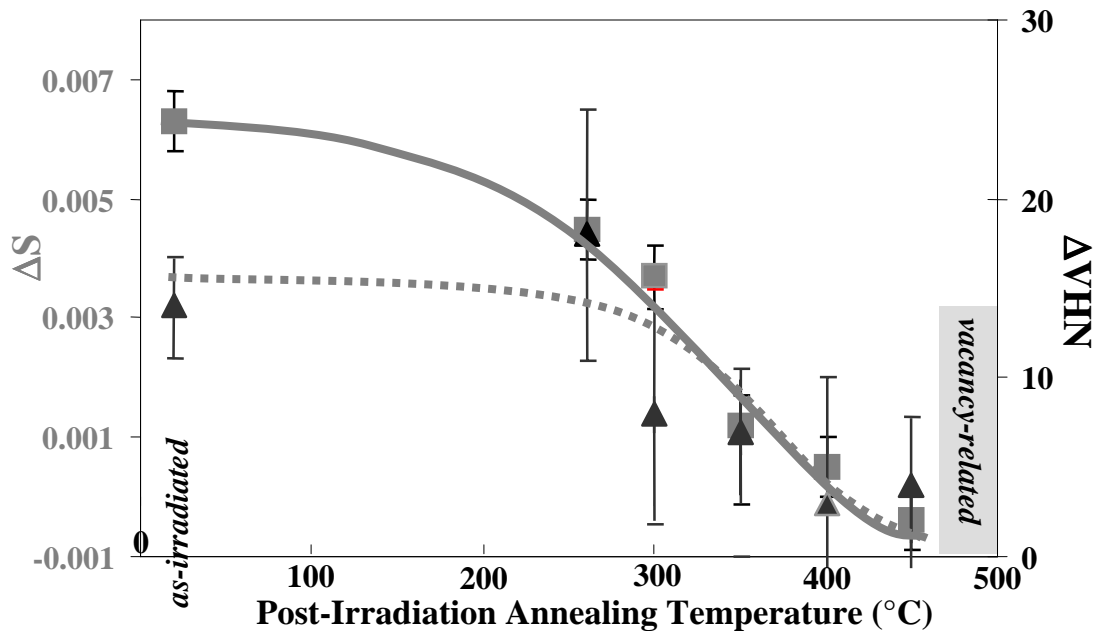


Figure 5 - Effect of PIA on the recovery of vacancy-related matrix damage (as measured by the PALA ΔS parameter - ■) and the recovery of irradiation-induced hardness (ΔVHN - ▲) for "superclean" steel 118K001 irradiated to 0.018 dpa. The parallel behavior of ΔS and ΔVHN suggests that the hardness increment was associated with vacancy-related damage.

“Superclean” Steel 118K001 (3.5 Ni – 0.02 Mn) irradiated to 0.018 dpa (high flux) - 3D-APFIM analysis of both the unirradiated archive and neutron-irradiated specimens revealed that Ni fluctuations (significance of 0.1%) were present in both materials. However, the χ^2 value increased from 67 for the archive specimen to 224 for the irradiated sample, indicating that irradiation did increase the magnitude of the Ni fluctuations. Contingency table analysis revealed that there was significant co-segregation between Ni and Si, with some co-segregation of Cu and Si (significance of 5%). Analysis of SANS data indicated an average feature size of ~1.4 nm, and number density of $\sim 6 \times 10^{23}/\text{m}^3$. The PALA ΔS parameter confirmed the presence of irradiation-induced vacancy-related matrix damage. An irradiation-induced hardness increase of ~14 VHN was measured. Post-irradiation annealing promoted recovery of both the vacancy-related matrix damage and the irradiation-induced hardness, with complete recovery at 400°C. Figure 5 shows the PALA ΔS parameter and the ΔVHN measurements as a function of PIA treatment for this steel.

Discussion

The 3D-APFIM, SANS, PALA and post-irradiation annealing data support the existence of two contributions to total irradiation damage in conventional A508 Gr 4N steels: irradiation-induced solute-related hardening features and vacancy-related matrix damage. It should be noted that the identification of two hardening components in irradiation damage does not imply that these two components are separate; rather, it is speculated that these solute fluctuations are directly associated with the vacancy-related damage. The primary argument for regarding the vacancy-related matrix damage as separate to the solute fluctuations arises from the PALA ΔS measurements as a function of PIA treatment. Eliminating the vacancy-related damage ($\Delta S \sim 0$) through post-irradiation annealing resulted in a reduction in hardness, but not complete recovery, in the conventional steels 207N947 and 124S285. Additional characterization of the post-irradiation annealed steel 207N947 confirmed that the Mn and Ni solute fluctuations were still present, indicating that the residual hardness was associated with the solute-related features. It was noted, however, that between the post-irradiation anneals at 350°C and 450°C, a reduction in the spatial correlation between Mn and Ni was detected. Furthermore, the dramatic reduction in scattering features as determined by SANS analysis of the post-irradiation annealed steel coincided with the similar reduction in the PALA ΔS parameter, providing evidence that the scattering features detected by SANS are vacancy-related.

The nature of the solute-related hardening features identified in this study are similar to the solute fluctuations reported by Hyde et al. in their analyses of irradiated low Cu 1.6 Ni- 1.5 Mn welds [11,12]. The statistical analysis of the 3D-APFIM data using composition frequency distributions and contingency table methodology [12,13] demonstrated the development of the Mn and Ni fluctuations, as well as the co-segregation of Mn and Ni that occurred during neutron irradiation. Also, significant co-segregation of Ni and Cu, Ni and Si, as well as Mn and Si was observed in the Steel

207N947 (0.1 wt.%Cu) irradiated to 0.018 dpa. This is consistent with published observations of a Ni-Cu effect in irradiation embrittlement [1-6]. Odette [14] has suggested that Cu clustering is the necessary and rate controlling process for the nucleation of Mn-Ni rich clusters in model steels. Indeed, Odette [14] speculated that the embrittlement associated with Mn-Ni rich clusters would be observed at higher doses than that due to “Cu clusters” but that, even at very low Cu levels, it might eventually equal or exceed the embrittlement produced by Cu-rich clusters in high Cu steels. No Ni-Cu cosegregation was observed in 0.03 wt.% Cu steel 118K001. This could suggest: 1) that there is a threshold below which Cu does not control the development of the solute fluctuations, or 2) that the low levels of Cu in the steel make it difficult to detect significant Cu solute fluctuations. It is noteworthy, however, that significant irradiation-induced Ni-Si, and Mn-Si cosegregation was detected by 3D-APFIM analysis despite the very low Si level in the high flux irradiated steels 207N947 and 124S285 (0.05 wt% and 0.03 wt.%, respectively).

The “superclean” 3.5 Ni steel contained Ni solute fluctuations, which became more significant as a result of neutron irradiation. This, coupled with the 3D-APFIM observations of Mn and Ni solute fluctuations and their co-segregation in the 0.3 Mn steels, indicates that the presence of Mn is essential for the irradiation-induced development of stable solute-related hardening features in the steel. This behavior was observed for both the low 0.05 Cu 124S285 and the higher 0.1 Cu 207N947 steels. In addition, comparison of the post-irradiation annealing behavior of the conventional (0.3 Mn) and “superclean” (0.02 Mn) A508 Gr 4N steels revealed that the conventional steels retained some residual irradiation-induced hardness whereas the 0.02 Mn steel experienced complete recovery after the anneal at 400°C. The complete recovery in irradiation damage as determined by PALA ΔS and ΔVHN measurements of the “superclean” 118K001 steel after the PIA treatment suggests that in the absence of Mn, high flux neutron irradiation may induce predominantly vacancy-related matrix damage leading to hardening.

Comparison of the low ($\sim 10^{-10}$ dpa/s) and high flux ($\sim 10^{-7}$ dpa/s) irradiated 124S285 specimens, although complicated by the differences in damage level and irradiation temperature, indicated that the low flux irradiation induced the formation of similar Mn and Ni solute fluctuations within the matrix as did the high flux irradiation. The low flux irradiation did not lead to spatial correlation of the Mn and Ni solute fluctuations whereas the high flux irradiation did. Furthermore, the post-irradiation annealing behavior of these specimens differed considerably. The high flux irradiated material experienced full recovery of the vacancy-related damage (via PALA ΔS parameter), but incomplete recovery in hardness. In contrast, the low flux irradiated specimen exhibited no significant difference in PALA ΔS parameter as a function of post-irradiation annealing, implying an absence of vacancy-related damage. Similarly, the hardness exhibited little change as a function of post-irradiation annealing. The hardness data for the high flux and low flux irradiated steel 124S285 samples as a function of post-irradiation annealing supports the two-component (solute-related hardening component + vacancy-related damage component) contribution of irradiation damage discussed earlier. It should also be noted that the magnitudes of the residual hardness following PIA are similar,

indicating that no significant flux effect was observed for solute-related hardening, although the high flux irradiation did promote detectable Mn-Ni co-segregation in the 0.3 Mn steels, which was not observed in the low flux irradiated steel.

The approximate magnitude of the two hardening components (solute-related + vacancy-related) identified for the high flux irradiated steels has been combined with the Charpy 47J transition temperature (TT_{47J}) data and composition data (Ni, Mn and Cu contents) in Figure 6. The previously reported TT_{47J} data and the ΔVHN data obtained in this study show that the increased levels of Ni do not lead to greater levels of embrittlement compared to lower Ni steels and other published “high Ni” (~1.4 to 2.6 wt.%) steel data [1-4,6]. It is important to note that the enhanced embrittlement reported for the high Ni steels and welds neglects the explicit identification of a Mn effect in the resultant embrittlement behavior. This is understandable in that most commercial steels and welds routinely contain Mn levels of ~1 to 1.5 wt%. The data presented in Figure 6, coupled with the results of the 3D-APFIM, SANS and PALA measurements, support a critical Mn contribution to the development of the irradiation-induced microstructure and irradiation damage behavior of high Ni steels. Thus, the observed microstructural development in the A508 Gr4N steels, “superclean” A508 Gr4N steel, and commercial high Ni welds and steels during neutron irradiation can be interpreted in terms of a Mn-Ni synergistic effect: the presence of Mn appears to stabilize the formation of the irradiation-induced solute-related hardening features in low alloy steels and welds containing low (0.1% or less) Cu.

It is possible to speculate on the role of solute fluctuation in the overall development of the hardening features formed as a result of neutron irradiation. At present, it cannot be unequivocally established from this work that the irradiation-induced solute fluctuations are the pre-cursor to solute-enriched clusters, but such a scenario is consistent with the previously reported observation for a conventional A508 Gr 4N steel with 0.08 wt.% Cu (irradiated at a low dose rate to 0.068 dpa) of well-defined “precipitate”-like features containing approximately 6% Cu (steel 123P171) [8].

Summary

The techniques of 3D-APFIM, SANS and PALA have been successfully employed to characterize the irradiation-induced microstructure of low Cu A508 Gr 4N forging steels. Two contributions to the observed irradiation-induced hardening were identified for high flux irradiation conditions: 1) solute-related hardening features (Mn and Ni solute fluctuations); and 2) vacancy-related matrix damage. 3D-APFIM and SANS characterization of post-irradiation annealed specimens confirmed that the Mn and Ni solute fluctuations contributed to the observed irradiation-induced hardness of the steel. Furthermore, characterization of the 3.5 Ni - 0.02 Mn superclean steel demonstrated that no stable solute-related hardening occurred during neutron irradiation. The results of this study suggest that Mn has a significant effect on the development of solute-related hardening features formed during neutron irradiation and the observed irradiation damage

behavior of high Ni low alloy steels. In addition, comparison of low flux and high flux irradiated steel revealed that the magnitude of solute-related hardening were similar, despite the nearly three orders of magnitude difference in flux. However, negligible vacancy-related damage was detected in the low flux irradiated steel.

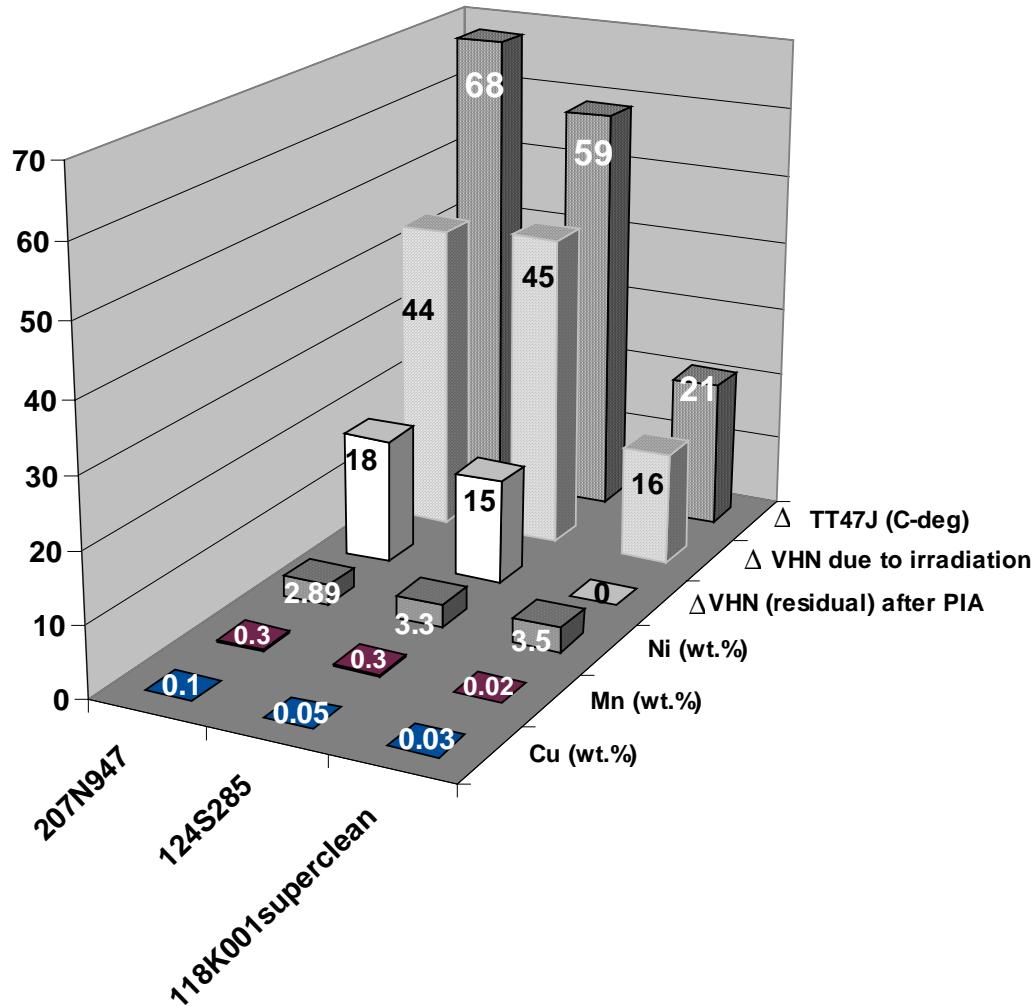


Figure 6 – Comparison of the TT_{47J} shift, irradiation-induced hardening increment, residual solute-related hardening after PIA treatment (to remove the vacancy-related damage), and composition of the conventional and superclean A508 Gr 4N steels irradiated under high flux conditions to 0.018 dpa (steel 124S285 – 0.017 dpa).

References

- [1] Odette, G.R., and Lucas, G.E., "The Effect of Nickel on Irradiation Hardening of Pressure Vessel Steels" *Effects of Radiation on Materials: 14th International Symposium (Vol. II)*, ASTM STP 1046, N. H. Packan, R. E. Stoller, and A. S. Kumar, Eds. American Society for Testing and Materials, Philadelphia, PA, 1990, 323-347.
- [2] Williams, T. J., Thomas, A. F., Berrisford, R. F., Austen, M., Squires, R. L., and Venables, J. H., "The Influence of Neutron Exposure, Chemical Composition and Metallurgical Condition on the Irradiation Shift of Reactor Pressure Vessel Steels" *Effects of Radiation on Materials: 11th International Symposium*, ASTM STP 782, H. Brager and J. Perrin, Eds., American Society for Testing and Materials, Philadelphia, PA, 1982, 343.
- [3] Williams, T. J., Ellis, D., Swan, D. I., McGuire, J., Walley, S. P., English, C. A., Venables, J. H. and Ray, P. H. N., "The Influence of Copper, Nickel and Irradiation Temperature on the Irradiation Shift of Low Alloy Steels," *Second International Symposium on Environmental Degradation of Materials in Nuclear Power Systems—Water Reactors*, ANS, La Grange Park, IL, 1986, 393.
- [4] Williams, T. J., Burch, P. R., English, C. A., and Ray, P. H. N., "The Effect of Irradiation Dose Rate and Temperature, and the Copper and Nickel Content on the Irradiation Shift of Low Alloy Steel Submerged Arc Welds," *Third International Symposium on Environmental Degradation of Materials in Nuclear Power Systems—Water Reactors*, AIME, Warrendale, PA, 1988, 121.
- [5] Buswell, J. T., Phythian, W. J., McElroy, R. J., Dumbill, S., Ray, P. H. N., Mace, J., and Sinclair, R. N., "Irradiation-Induced Microstructural Changes, and Hardening Mechanisms, in Model PWR Reactor Pressure Vessel Steels," *Journal of Nuclear Materials*, 225 (1995) 196-214.
- [6] Kryukov, A. M., Nikolaev, Y. A., Nikolaeva, A. V., "Behavior of Mechanical Properties of Nickel-Alloyed Reactor Pressure Vessel Steel under Neutron Irradiation and Post-Irradiation Annealing," *Nuclear Engineering and Design*, 186 (1998) 353-359.
- [7] Miller, M. K., Pareige, P. and Burke, M. G., "Understanding Pressure Vessel Steels: An Atom Probe Perspective" *Materials Characterization*, 44 (2000) 235.
- [8] Burke, M. G., Stofanek, R. J., Hyde, J. M., English, C. A., Server, W. L., "Characterization of Irradiation Damage in A508 Class 2 and Class 4 Forging Steels," *10th International Symposium on Environmental Degradation of Materials in Nuclear Power Systems—Water Reactors*, G. Was and L. Nelson, Eds., NACE, 2002.
- [9] Stofanek, R. J., Poskie, T. J., Li, Y. Y., Wire, G. L., "Irradiation Damage Behavior of Low Alloy Steel Wrought and Weld Materials," *6th International Symposium on Environmental Degradation of Materials in Nuclear Power Systems—Water Reactors*, TMS, Warrendale, PA, 1993, 757.
- [10] Stofanek, R. J., Li, Y. Y., Burke, M. G., Matuszyk, K., "Irradiation Embrittlement of High Strength Low Alloy Steels Containing About 3.3% Ni," *10th International*

Symposium on Environmental Degradation of Materials in Nuclear Power Systems—Water Reactors, G. Was and L. Nelson, Eds., NACE, 2002.

- [11] Hyde, J. M., and English, C. A., “An Analysis of the Structure of Irradiation-Induced Cu-Enriched Clusters in Low and High Nickel Welds”, *Microstructural Processes in Irradiated Materials – 2000: Materials Research Society Symposium Proceedings Volume 650*, G. E. Lucas, L.L. Snead, M. A. Kirk and R. G. Elliman, Eds., MRS, Warrendale, PA, 2001, R6.6.1-12.
- [12] Hyde, J. M., Ellis, D., English, C. A., and Williams, T. J., “Microstructural Evolution in High Ni Submerged Arc Welds,” *Effects of Radiation on Materials: 20th International Symposium, ASTM STP 1405*, S. T. Rosinski, M. L. Grossbeck, T. R. Allen, and A. S. Kumar, Eds., American Society for Testing and Materials, West Conshohocken, PA, 2001, 262-288.
- [13] Miller, M. K. and Smith, G. D. W., *Atom Probe Microscopy: Principles and Applications in Materials Science* (Materials Research Society, Pittsburgh) 1989.
- [14] Odette, G. R., “Radiation-Induced Microstructural Evolution in Reactor Pressure Vessel Steels” *MRS Symposium Proceedings, Vol. 373* (1995) 137-148.